Environmental Science and Pollution Research (2023) 30:123751–123769
https://doi.org/10.1007/s11356-023-30805-0

RESEARCH ARTICLE

Functional Ag-EDTA-modified MnO_2 nanocoral reef for rapid removal of hazardous copper from wastewater

Omnia I. Ali[1] · **Ahmed B. Azzam**[1]

Received: 8 September 2023 / Accepted: 27 October 2023 / Published online: 22 November 2023

Abstract

A novel MnO_2@EDTA-Ag nanocoral reef was constructed via a simplified redox reaction followed by EDTA and Ag nanoparticles impregnation to capture hazardous copper (II) from wastewater. A comprehensive characterization of the synthesized materials was conducted. The morphology of MnO_2@EDTA-Ag in the form of a nanocoral reef was constructed of two-dimensional nanoplatelets and nanorod-like nanostructures. The optimal adsorption conditions proposed by the Plackett–Burman design (PBD) that would provide a removal % of 99.95 were pH 5.5, a contact time of 32.0 min, a Cu(II) concentration of 11.2 mg L^{-1}, an adsorbent dose of 0.05 g, and a temperature of 40.3 °C. The loading of Ag nanoparticles onto MnO_2@EDTA improved the adsorption capability of MnO_2@EDTA-Ag. Additionally, the recyclability of MnO_2@EDTA-Ag nanocoral reef was maintained at 80% after three adsorption–desorption cycles, and there was no significant change in the XRD analysis before and after the recycling process, implying its stability. It was found that nanocoral reef-assisted EDTA formed a chelation/complexation reaction between COO^- groups and C–N bonds of EDTA with Cu(II) ions. In addition, X-ray photoelectron spectroscopy (XPS) and Fourier transform infrared spectroscopy (FTIR) analysis proved the synergistic effect of the electrostatic interaction and chelation/complexation was responsible for the removal mechanism of Cu(II). Also, the results demonstrated no significant variation in MnO_2@EDTA-Ag removal efficiency for all the tested real water samples, revealing its efficacy in wastewater treatment. Therefore, the current study suggests that MnO_2@EDTA-Ag has substantial potential to be used as a feasible adsorbent for probable hazardous metals remediation.

Keywords MnO_2 nanostructures · EDTA-impregnation · Ag nanoparticles · Copper removal · Plackett–Burman design

Introduction

One of the most serious challenges facing the globe today is water scarcity, and resource depletion in some regions is leading to significant international conflict and human suffering (Asim et al. 2021; Lee et al. 2021). Wastewater treatment has been recognized as an essential concern over the past few decades, along with the growing industrialization of society (Fu et al. 2019; Elfiad et al. 2020). Heavy metal ions are frequently released by industrial waste, particularly in the metal coating, leather tanning, and petroleum refining industries. Clean water technologies have faced a major barrier for removing highly hazardous and ultra-dilute contaminants of concern. Due to its hazardous and non-biodegradable properties, copper is one of the most prevalent heavy metal contaminants in urban and agricultural water (Hama Aziz et al. 2023). Copper is derived from numerous industrial wastewaters, such as printed circuit boards (PCBs) and electroplating effluent (Chen and Xie 2020; Duan et al. 2023). The World Health Organization (WHO) has established a limit of 2 mg L^{-1} for copper ions in drinking water; however, the United States Environmental Protection Agency (USEPA) has set an allowed maximum of 1.3 mg L^{-1} for copper ions in industrial effluents (Al-Saydeh et al. 2017). A variety of physicochemical and biological methods, including electrodialysis, coagulation and flocculation, membrane filtration, and adsorption, have been used to decontaminate water that has been contaminated with potentially dangerous metals (Dastkhoon et al. 2018; Guo et al. 2021; Shi et al. 2021; Kuang et al. 2022). However, all approaches have deficiencies, such as the requirement for extensive amounts of chemicals

Responsible Editor: Tito Roberto Cadaval Jr

✉ Omnia I. Ali
omniaali@science.helwan.edu.eg;
omniaibrahim95@gmail.com

[1] Chemistry Department, Faculty of Science, Helwan University, Cairo 11795, Egypt

and energy, limited separation selectivity, partial pollutant removal, and the production of sludge that must be safely disposed of (Markovski et al. 2014). Adsorption, one of the many methods for removing metal ions from water, is a quick and affordable process that makes it simple to regenerate and recover the separation medium (Hasanpour and Hatami 2020).

Owing to their enormous surface area, varied morphologies, and significant activity, nanosized metal oxides (NMOs) have a promising capacity to remove heavy metals from aquatic environments (Shi et al. 2021). Moreover, with their excellent adsorption capacity, selectivity, and oxidation abilities, nanostructured manganese oxides (MnO_2) have been extensively employed for the removal of hazardous pollutants (Wei et al. 2019; Husnain et al. 2020). One of the most diverse groups of porous materials, MnO_2 includes nanorods, nanowires, nanoflowers, nanotubes, nanoparticles, and nanosheets among its many different structures and morphologies (Mallakpour and Motirasoul 2017). It has numerous crystallographic forms, such as α, β, γ, δ, ε, and λ-type, that are different in the spatial arrangement of MnO_6 octahedral units (Ghosh 2020). Due to their exceptional structural flexibility and new physical and chemical properties, manganese dioxides and their derivative compounds have received a lot of attention. Therefore, they can be utilized in many scientific and industrial applications, such as fuel cells, energy storage devices (supercapacitors and rechargeable batteries), catalysis, sensors, and adsorbents (Zhang et al. 2015; Zhao et al. 2017; Liu et al. 2018; Husnain et al. 2020; Bigiani et al. 2020; Hao et al. 2020; Asim et al. 2021; Claros et al. 2021). However, MnO_2 nanostructures have a significant tendency to adhesion and aggregation because of their high energy surface, small size, and electrostatic forces that limit their performance. Surface enhancements that are chemical and physical can solve this problem (Mallakpour and Motirasoul 2017). Therefore, we employed EDTA to modify the surface of MnO_2 with the coordination of carboxylic groups (–COOH) to the surface of MnO_2. EDTA is a metal-chelating agent with high intrinsic selectivity that is commonly attached to substrate surfaces for application. Chen et al. prepared Fe_3O_4-MnO_2-EDTA magnetic nanoparticles for targeted Cu(II) adsorption in a complex system (Chen and Xie 2020). EDTA-modified composites have comparable separation challenges as traditional adsorbents. However, common chelating agent EDTA has the ability to form stable chelates with metal ions and has good degradability in certain environmental systems, which can prevent secondary pollution (Repo et al. 2010; Panahandeh et al. 2021). Noble metals have recently received a lot of attention for their outstanding adsorption abilities. Due to their unique qualities, such as closely packed structure, varied crystallographic facets, and high surface-to-volume ratio, Ag nanoparticles (NPs) have been widely used as a possible adsorbent for industrial applications (Song et al. 2016; Vicente-Martínez et al. 2020). However, its reusability in large-scale wastewater treatment applications is constrained by NPs aggregation and challenging recovery. Therefore, employing effective assistance for Ag NPs may help in resolving these issues. An interesting candidate for use as an adsorbent material is the direct incorporation of Ag NPs on other active materials such as MnO_2. However, the direct immobilization of Ag NPs onto active materials, such as MnO_2, causes repulsive forces that need to be overcome to address stability. The issue of repulsive forces can be solved by incorporation an organic buffer layer between the two active materials, which will also provide a strong synergy in the hybrid structure, allowing it to be employed as an efficient adsorbent (Sharif et al. 2019).

Herein, a novel MnO_2@EDTA-Ag nanocoral reef was effectively synthesized via a facile redox reaction followed by impregnation with EDTA and silver nanoparticles for rapid removal of hazardous copper (II) from real water samples. The dissolution of the MnO_2 adsorbent was avoided by impregnation with EDTA and Ag nanoparticles. Therefore, the feasibility of our strategy provides essential support for stability evaluation towards Cu(II) ions with acceptable adsorption properties. First, coral reef-like MnO_2 nanoparticles were prepared via a rapid redox reaction between $KMnO_4$ and Mn(II) sulfate. The dissolution of MnO_2 adsorbent was avoided by impregnation with EDTA and Ag nanoparticles as well. Statistical methods of experimental design, including factorial design and response surface analysis, have been employed in different methods for heavy metals' removal because of their ability to reduce the limitations of the time-consuming single-factor conventional and classical methods. For example, the Plackett–Burman design is a quick and useful screening technique to find the significant parameters amid a large number of variables, ensuring that each parameter is well understood, and saving time as well (Taylor et al. 2012; El-naggar et al. 2018). Therefore, the influences of all studied parameters on the removal efficiency of Cu(II) using MnO_2@EDTA-Ag were investigated systematically using the Plackett–Burman design. A statistical analysis of the obtained results was carried out using ANOVA to evaluate the inference and impact of the studied parameters on copper removal. In addition, the impact of operating parameters, such as the initial pH, contact time, dose of adsorbent, initial metal concentration, temperature, and interfering ions towards Cu(II) removal was explored by adopting batch mode. To further assess the sorption behavior of MnO_2@EDTA-Ag, the kinetics, rate-controlling mechanisms, isotherms, and thermodynamic characteristics of the sorption process have also been examined. Additionally, the desorption study, stability evaluation, and feasible mechanistic pathway for Cu(II) removal were elucidated.

Experimental

All materials and the characterization methodologies are provided in the electronic supplementary information (ESI).

Synthesis of MnO_2 nanostructures

A simple, ultrafast, economical, and environmentally friendly redox reaction was developed for the construction of nanocoral reef-like MnO_2. In a 500-mL beaker, 4.61 g of $MnSO_4$ was combined with 100 mL of isopropyl alcohol (IPA). The solution was vigorously stirred while being heated to around 60 °C. After being thoroughly dissolved in 150 mL of double-distilled water, 3.00 g of $KMnO_4$ was quickly added to the previously mentioned boiling solution while being stirred for 10 min. Immediately, a significant amount of brown-black precipitate was collected. After being centrifuged, the mixture was cleansed with double-distilled water and oven-dried for 6 h at 90 °C. Under the same conditions, various solvents were used to create additional MnO_2 structures. Typical solvents included glycerol and ethylene glycol.

Synthesis of Ag-EDTA-modified MnO_2 nanostructures

The above-obtained brown-black precipitate MnO_2 (100 mg) prepared by isopropyl alcohol (IPA) as a solvent was dispersed in 20 mL H_2O and followed by 100 mg of EDTA. The mixture was mixed for 2 h and then agitated for 48 h at room temperature. The resulting EDTA-modified MnO_2 nanostructures were labelled as MnO_2@EDTA. A simple sonochemical method was developed to construct embedded Ag nanoparticles on MnO_2@EDTA. In order to create the Ag–NH_4^+ solution, 150 mg of $AgNO_3$ was combined with 25 mL of NH_4OH (5%) in 150 mL of water. Afterward, 150 mL of Ag–NH_4^+ solution was sonicated with 50 mg of MnO_2@EDTA for 10 min at room temperature. Finally, the grayish-black solid product (MnO_2@EDTA-Ag) was centrifugated, washed with dilute HNO_3, and double-distilled water several times, then dried at a temperature of 70 °C.

Statistical experimental design

For studying Cu(II) removal using MnO_2@EDTA-Ag, the removal percentage of metal could depend on the medium pH, the initial Cu(II) concentration (C_o), the contact time (t), the adsorbent dose (m), and the temperature. Plackett–Burman design was employed to determine the significant parameters for Cu(II) removal. The low and high levels are given in Table 1. Design expert statistical software program, version 12, was employed for the experimental design and data statistical analysis.

Adsorption experiments

Batch adsorption experiments were conducted at a constant rate of 150 rpm in a thermostatic shaking water bath (AHAAM, Egypt). The impacts of several parameters were studied, such as initial pH (2–6), contact time (1–120 min), initial Cu(II) concentration (10–50 mg L^{-1}), the adsorbent dose (0.001–0.1 g), and temperature (25–55 °C) using 10 mL of Cu(II) solutions. The pH values of the copper solutions were altered as required through the addition of drops of HCl (0.1 mol L^{-1}) or NaOH (0.1 mol L^{-1}). The values of the point of zero charges (pH_{PZC}) of the prepared adsorbents were calculated using the salt addition method (Bakatula et al. 2018). After a measured time interval, samples were taken out and filtered through a membrane syringe filter (0.22 µm) to be analyzed to determine the residual Cu(II) concentration using the modified sodium diethyldithiocarbamate method (Ali and Mohamed 2017).

Table 1 Levels of the parameters tested in Plackett–Burman design

Parameter	Symbol	Level	
		Low (− 1)	High (+ 1)
pH	A	2	6
Time (min)	B	1	60
Concentration of Cu(II) (mg L^{-1})	C	10	50
Adsorbent dose (g)	D	0.001	0.1
Temperature (°C)	F	25	55

The removal efficiency ($R\%$) and the amount of Cu(II) adsorbed (q_e, mg g^{-1}) were calculated using the following equations. (Mozaffari et al. 2020b, c):

$$R\% = \frac{\left(C_o - C_e\right)}{C_o} \times 100 \quad (1)$$

$$q_e\left(\text{mg g}^{-1}\right) = \frac{\left(C_o - C_e\right) \times V}{m} \quad (2)$$

where C_o and C_e (mg L^{-1}) represent the initial and equilibrium copper concentrations, respectively; V is the volume (L) of the copper solution, and m denotes the mass (g) of the adsorbent.

Desorption and reusability

After adsorption of 10 mL Cu(II) (10 mg L^{-1}) using 0.01 g of MnO_2@EDTA-Ag, the loaded adsorbent was filtered and dried. The adsorbed Cu(II) was desorbed using different concentrations (0.001, 0.005, and 0.01 mol L^{-1}) of different acids (HCl, HNO_3, and H_2SO_4). The desorbed Cu(II) was separated and analyzed as described in the "Adsorption experiments" section. Desorption efficiency (E_{Des}) was estimated using Eq. (3) (Ali et al. 2020):

$$E_{\mathrm{Des}} = \frac{D_{\mathrm{Des}}}{A_{\mathrm{Ads}}} \times 100 \quad (3)$$

where the amounts of adsorbed and desorbed Cu(II) are represented by A_{Ads} and D_{Des}, respectively. The regenerated adsorbent was employed in the following adsorption tests for reusability, and the adsorption–desorption cycle was repeated with the same sample. The produced adsorbent's ability to capture Cu(II) ions from a variety of real water samples was next tested analytically. Several water samples were used, including tap water, groundwater, and Nile water.

Results and discussion

Characterization

The XRD patterns of the MnO_2, MnO_2@EDTA, and MnO_2@EDTA-Ag samples are shown in Fig. 1 a. The figure shows that all of the samples had heterogeneous crystalline forms of manganese oxide: a major phase of γ-MnO_2 with a minor phase of β-MnO_2. The diffraction peaks at about 21.87°, 37.43°, 41.97°, and 55.56° corresponded to (120), (131), (300), and (160) lattice planes of γ-MnO_2 (JCPDS 14–0644). On the other hand, the diffraction peak at about 28.5° for the MnO_2 sample corresponded to the reflection plane of (110) of a pyrolusite-type (β-MnO_2) of manganese oxide (JCPDS 24–0735) (Devaraj and Munichandraiah 2008; Bai et al. 2016; Raheem and Al Sammarraie 2020; Sun et al. 2020). It can be observed that there is no significant difference in the XRD pattern of MnO_2@EDTA upon the modification of the MnO_2 sample with EDTA, demonstrating that the phase structure was almost completely conserved. However, with the incorporation of Ag nanoparticles, it can be seen that the peaks became sharper and more intense (Fig. 1b), reflecting the higher crystallinity of MnO_2@EDTA-Ag sample. In addition, the XRD pattern of MnO_2@EDTA-Ag lacked the expected Ag diffraction peaks, which may be attributable to the great dispersion of Ag nanoparticles.

The surface functional groups of MnO_2, MnO_2@EDTA, and MnO_2@EDTA-Ag nanocoral reef were verified by FT-IR spectra as shown in Fig. 2. The peaks located around 500 and 720 cm^{-1} are associated with the Mn–O vibration of [MnO_6] octahedra (Asim et al. 2021). A new peak at 1409 cm^{-1} is observed in MnO_2@EDTA and MnO_2@EDTA-Ag samples, and it is attributed to the symmetric stretching vibration of C–N bonds and COO^- groups derived from EDTA (Chen and Xie 2020). This new peak is absent in the MnO_2 sample, indicating that EDTA was successfully anchored on MnO_2@EDTA. The non-existence of this peak in MnO_2 sample is evidence of the successful anchoring of EDTA in the MnO_2@EDTA sample. In addition, a small peak that appeared at 450 cm^{-1} is assigned to Ag, confirming that Ag nanoparticles have been successfully embedded into MnO_2@EDTA (Sharif et al. 2019). The bending vibrations of the –OH groups associated with the Mn atoms appeared at a peak of 1634 cm^{-1} (Dinh et al. 2020). The broad vibration band around 3382 cm^{-1} represents O–H stretching vibration, which is from water molecules that are physically adsorbed to the surface of samples (Revathi and Kumar 2017; Cao et al. 2021).

The surface morphologies of MnO_2@EDTA and MnO_2@EDTA-Ag structures were characterized by FESEM. As displayed in Fig. 3a–b, MnO_2@EDTA shows a nanocoral reef composed of a two-dimensional nanoplatelet structure with the formation of some nanorods out of the plate structure. Figure 3c–d clearly show the in situ deposition of Ag (NPs) on the surface of the MnO_2@EDTA nanocoral reef. The

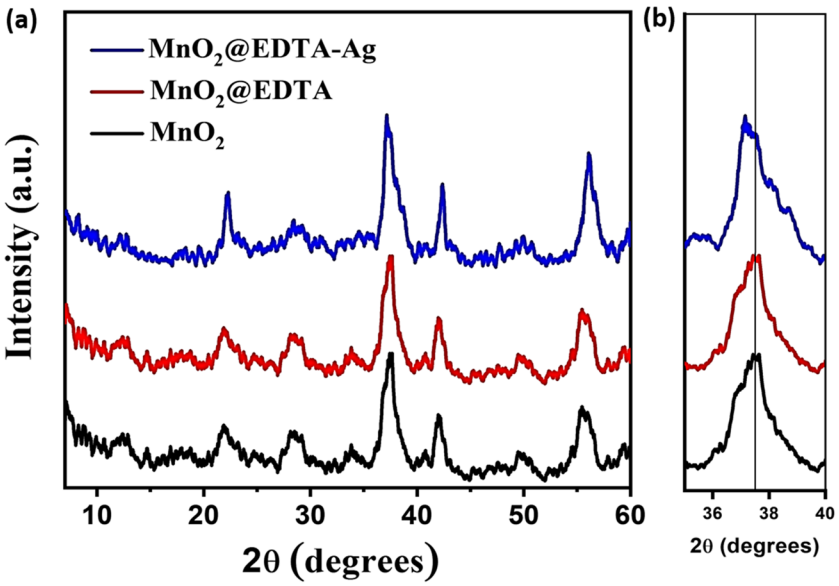

Fig. 1 XRD patterns of MnO_2, MnO_2@EDTA, and MnO_2@EDTA-Ag nanocoral reef

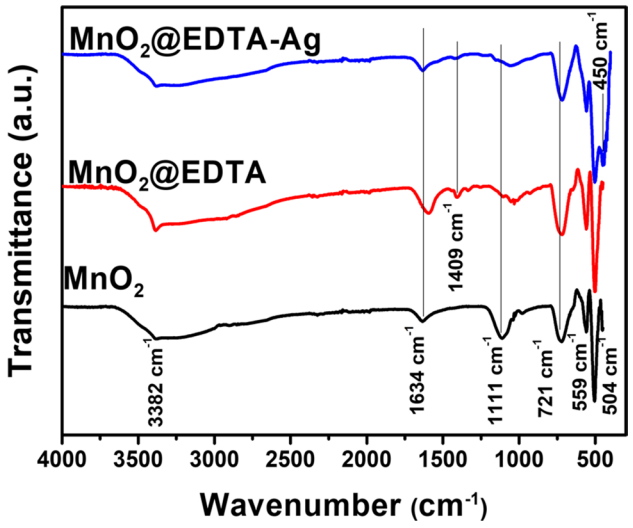

Fig. 2 FTIR spectra of MnO_2, MnO_2@EDTA, and MnO_2@EDTA-Ag nanocoral reef

elemental mapping analysis (Fig. 3e–j) indicated that Mn, O, C, N, and Ag elements were homogeneously distributed in the hybrid structure. The EDX spectrum of MnO_2@EDTA-Ag is shown in Fig. 3g, and the elemental composition confirms the existence of Mn, O, C, N, and Ag elements. In the meantime, the TEM images (Fig. 4a–b) also confirmed that the obtained MnO_2@EDTA-Ag was a nanocoral reef composed of two-dimensional nanoplatelet with nanorod-like structure, which was the same as the SEM results. The average diameter of a nanoplatelet is 60 nm, and the diameters of nanorods are about 10 to 80 nm and 200 nm in length. In addition, the embedded Ag NPs were observed and attached to the surface nanorods (Fig. 4b). HRTEM image (Fig. 4c) of MnO_2@EDTA-Ag nanocoral reef exhibited lattice fringes of 0.24 and 0.31 nm. These spacings are related to the (131) lattice plane of the γ-MnO_2 phase and the (110) lattice plane of the β-MnO_2 nanostructures, as shown in Fig. 4c. It can be concluded that the Ag NPs were successfully immobilized on the MnO_2@EDTA nanocoral reef to form a hybrid structure. Figure 4 d illustrates the SAED pattern of the MnO_2@EDTA-Ag nanocoral reef, which demonstrates the polycrystalline nature of the hybrid structure.

Statistical experimental design

Plackett–Burman design (PBD) using two-level factors was utilized to analyze the removal of Cu(II) ions employing MnO_2@EDTA-Ag taking into consideration different parameters: pH (A), contact time (B), initial Cu(II) concentration (C), adsorbent dose (D), and temperature (E). Table 2 summarizes the different operating parameters along with the experimental results of *R*% for Cu(II) removal using MnO_2@EDTA-Ag according to PBD experiments. The data listed in the table indicated a substantial variation in Cu(II) removal efficiency. The lowest *R*% of 8.34% was achieved using a MnO_2@EDTA-Ag dose of 0.005 g, 1 min as contact time, 50 mg L^{-1} Cu(II), pH 3, and at 55 °C. In contrast, the highest *R*% (95%) was reached with a MnO_2@EDTA-Ag dose of 0.05 g, 90 min as a contact time, 10 mg L^{-1} Cu(II), pH 6, and at 55 °C. The residuals between the practical (actual) and predicted (model) values were found to be small, indicating that both the observed and predicted responses had satisfactory agreement.

Analysis of variance (ANOVA) was employed to assess the appropriateness of the model. The ANOVA of R% of Cu(II) using MnO_2@EDTA-Ag is exhibited in Table 3. The model is highly significant in this study, as shown by the *F* value of 273.61, and there was only a 0.03% possibility that the results were only due to noise. The correlation coefficient (R^2) manipulated to reveal the relationship between the experimental (actual) and predicted responses was 0.9986, as confirmed by the model. This implies that the process parameters analyzed justify 99.86% of the removal efficiency variability. Moreover, as displayed in the table, the value of the predicted R^2 (0.9791) is in acceptable agreement with the adjusted R^2 (0.9950), i.e., the deviation is < 0.2. Also, model terms with *P*-values < 0.05 imply that they are statistically significant. The dose (D) of MnO_2@EDTA-Ag was the most significant parameter affecting Cu(II) removal, followed by Cu(II) concentration (C) > pH (A) >> time (B) and their interactions (AB and BC). On the other hand, temperature (E) and interaction (CE) had no significant impact on Cu(II) removal. As demonstrated in Table 3, the respective contributions of the investigated parameters, including pH, time, Cu(II) concentration, adsorbent dose, and temperature, were 31.7, 30.51, 25.17, 12.44, and 0.18%, respectively. In addition, a Pareto chart was employed to affirm the impact of each parameter on Cu(II) removal (Fig. 5a). As demonstrated, pH and adsorbent dose had positive effects on the Cu(II) removal efficiency, whereas time and Cu(II) concentration had negative effects. The following equation can be utilized to figure out the model equation of R% for copper removal:

$$\begin{aligned} R\% = {} & 57.77 + 9.59 \times \mathrm{pH} - 2.09 \times \mathrm{Time} - 15.15 \\ & \times \mathrm{Conc.} + 19.72 \times \mathrm{Dose} + 1.02 \times \mathrm{Temp.} \\ & - 3.00 \times \mathrm{pH} \times \mathrm{Time} + 3.30 \times \mathrm{Time} \times \mathrm{Conc.} \\ & - 1.69 \times \mathrm{Conc.} \times \mathrm{Temp.} \end{aligned} \quad (4)$$

Figure 5b displays the plot between the actual values and predicted values of the removal efficiency of Cu(II). As demonstrated, both values are in reasonable agreement.

In this investigation, there was just one response taken into account, and the objective was to achieve the highest possible *R*%. The input parameters were each given values that were within a predetermined range (Fig. 6), while the

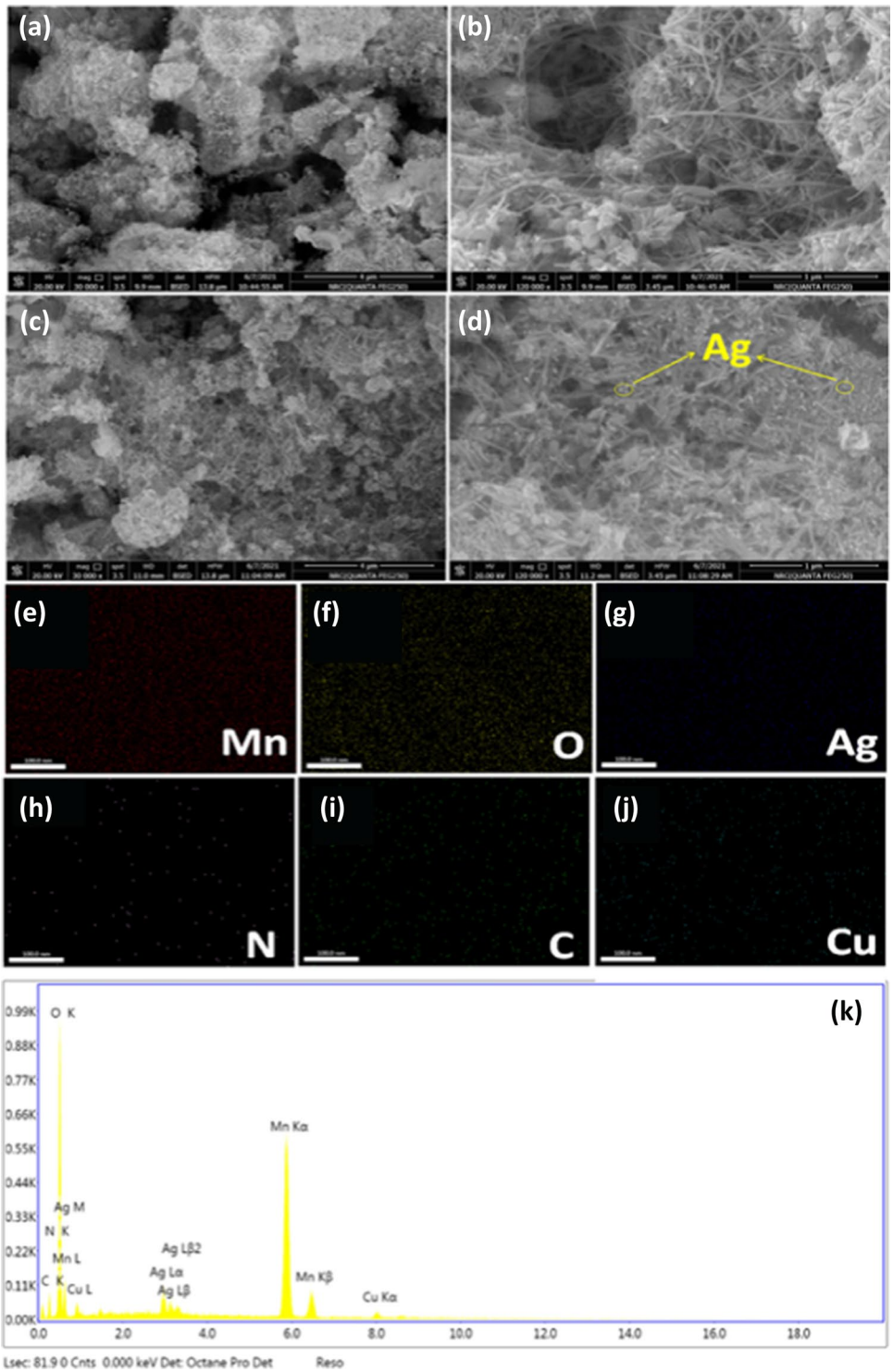

Fig. 3 **a**–**b** FESEM images of MnO_2@EDTA nanocoral reef; **c**–**d** MnO_2@EDTA-Ag nanocoral reef; **e**–**j** elemental mapping of MnO_2@EDTA-Ag nanocoral reef after copper removal showing Mn, O, Ag, N, C, and Cu; **k** EDX of MnO_2@EDTA-Ag nanocoral reef

response (*R*%) was considered to achieve a maximum. The ramp desirability is shown in Fig. 6, which was generated using a total of 112 starting points using numerical optimization using the Design Expert software. As observed, the experimental conditions of pH = 5.5, time = 32.0 min, Cu(II) conc. = 11.2 mg L^{-1}, dose = 0.05 g, and temp. = 40.3 °C would achieve a *R*% of 99.95 and desirability of 1.000.

Adsorption studies

Effect of the solvent type

To investigate how the kind of solvent affects the prepared adsorbents' ability to adsorb, MnO_2 nanostructures were fabricated using different solvents, including isopropyl alcohol,

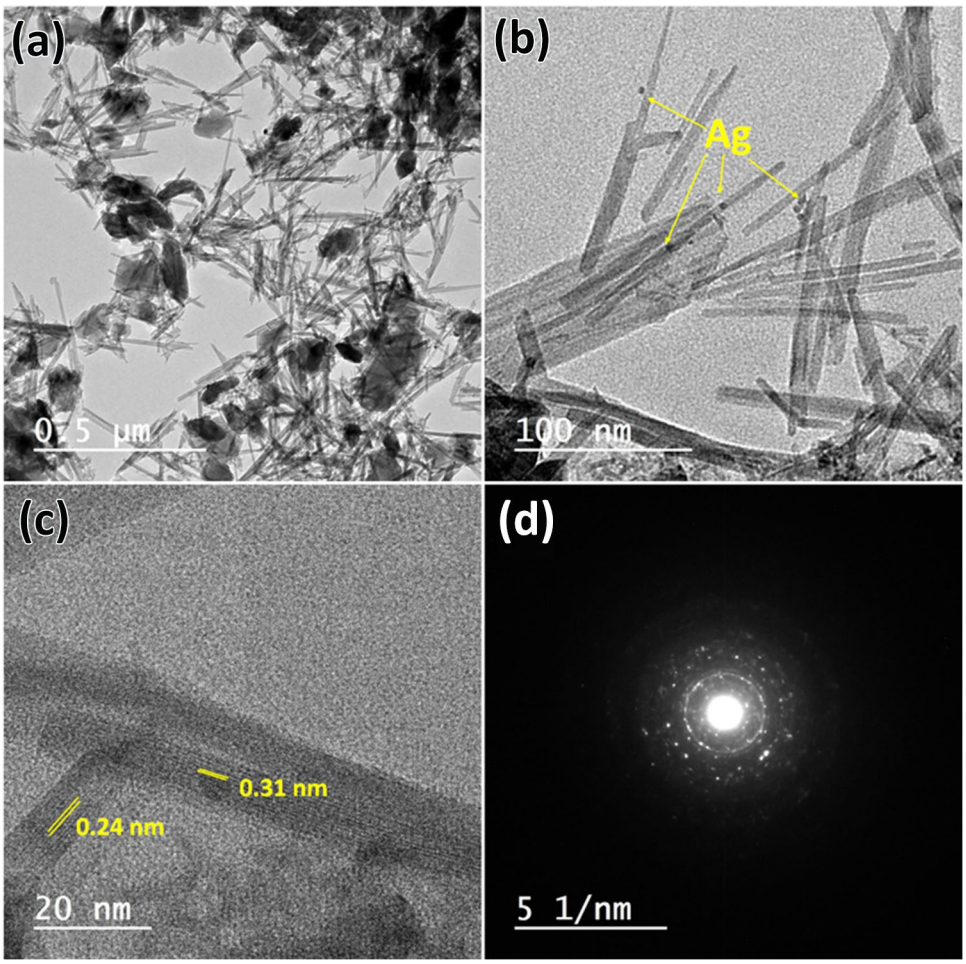

Fig. 4 **a**–**b** TEM images, MnO_2@EDTA-Ag; **c** HRTEM; **d** SEAD pattern

Table 2 Results of Cu(II) removal using MnO_2@EDTA-Ag using Plackett–Burman design

Run no	pH	Time (min)	Conc. (mg L^{-1})	Adsorbent dose (g)	Temp. (°C)	Experimental *R*%	Predicted *R*%	Residuals
1	6	90	10	0.005	25	51.59	51.68	−0.138
2	3	90	50	0.005	55	15.8	16.86	−1.039
3	6	1	50	0.05	25	73.34	74.40	−1.039
4	3	1	10	0.005	25	42.99	43.29	−0.214
5	3	90	10	0.05	55	85	83.38	1.586
6	6	90	50	0.005	25	33	31.38	1.586
7	3	1	10	0.05	25	83.12	82.73	0.378
8	6	90	10	0.05	55	95	96.54	−1.605
9	3	1	50	0.005	55	8.34	8.43	−0.138
10	3	90	50	0.05	25	57.1	57.66	−0.447
11	6	1	50	0.05	55	74.2	73.05	1.201
12	6	1	10	0.005	55	73.8	73.89	−0.138

Table 3 Analysis of variance for the experimental results of the PBD

Source	Sum of squares	df*	Mean squares	*F*-value	*p*-value	Contribution %
%Model	8603.16	8	1075.39	273.61	0.0003	
A-pH	734.98	1	734.98	187.00	0.0008	12.27
B-Time	43.65	1	43.65	11.10	0.0446	0.73
C-Conc	2293.71	1	2293.71	583.58	0.0002	38.29
D-Dose	2745.49	1	2745.49	698.52	0.0001	45.83
E-Temp	8.26	1	8.26	2.10	0.2431	0.14
AB	60.20	1	60.20	15.32	0.0297	
BC	72.71	1	72.71	18.50	0.0231	
CE	19.10	1	19.10	4.86	0.1147	

**df*: degrees of freedom, $R^2 = 0.9986$, adjusted $R^2 = 0.9950$, predicted $R^2 = 0.9791$

glycerol, and ethylene glycol, where they were denoted as IPA, EG, and GL, respectively. These materials were independently used to prepare MnO_2@EDTA structures and were labelled IPA-EDTA, EG-EDTA, and GL-EDTA, respectively. These prepared materials were employed to capture Cu(II) ions, and the results are illustrated in Fig. S1. Obviously, there is a slight difference in their removal efficiencies towards Cu(II) ions, where MnO_2 and MnO_2@EDTA prepared via isopropyl alcohol exhibited the highest removal percentage. Therefore, MnO_2@EDTA-based isopropyl alcohol was used to prepare MnO_2@EDTA-Ag, and both were employed in the succeeding investigations.

Effect of initial pH

Figure 7a illustrates the effect of pH on the Cu(II) adsorption onto the MnO_2@EDTA and MnO_2@EDTA-Ag nanocoral reef at initial pH values that varied from 2 to 6. Furthermore, the pH_{PZC} values for MnO_2, MnO_2@EDTA, and MnO_2@EDTA-Ag nanocoral reef (Fig. 7b) were calculated, and they were discovered to be 4.7, 5.3, and 4.3, respectively. It can be noted that as the pH of the Cu(II) solution was raised from 2 to 6, the removal efficiency of the two adsorbents gradually increased. The trend can be interpreted in terms of the electronegativity property of the adsorbents' surfaces. At low pH values, extra protons and Cu(II) ions competed for the binding sites of the MnO_2@EDTA and MnO_2@EDTA-Ag nanocoral reef, resulting in low removal efficiency. As pH values increased, the functional groups on the adsorbents were deprotonated, thereby rendering them more accessible to adsorb Cu(II) ions through electrostatic attraction forces. Based on these observations and the pH_{PZC} values, it can be presumed that electrostatic attraction forces were not the only mechanism for Cu(II) adsorption on the prepared adsorbents. It is possible that several sorption processes, including surface complexation, ion exchange, and precipitation, may be involved in addition to the electrostatic attraction process. These processes have been reported before (Touihri et al. 2021). Hence, pH 6 was utilized in the experiments that followed.

Effect of contact time and initial concentration

Figure 7 c shows the removal efficiency (*R*%) of Cu(II) of MnO_2@EDTA and MnO_2@EDTA-Ag nanocoral reef as a function of time and constant pH 6. Initially, the Cu(II) adsorption onto MnO_2@EDTA and MnO_2@EDTA-Ag was fast. In the first 5 min, 47.4% and 82.3% of Cu(II) were adsorbed onto MnO_2@EDTA and MnO_2@EDTA-Ag, respectively. Further, the uptake % of Cu(II) increased gradually up to 120 min with the increasing extension of contact time between adsorbent and adsorbate and afterward sustained a plateau with 86% and 98% removal using MnO_2@EDTA and MnO_2@EDTA-Ag, respectively. The rapid initial adsorption rate is responsible for the considerable number of accessible active sites in terms of functional groups and pores on the surface of nanocoral reef in the early stages of the adsorption process. The Cu(II) molecules build up on the surface of the adsorbent as the process of adsorption progresses, blocking molecules from diffusing into the pores and causing a slow adsorption rate (Choudhary et al. 2020). In addition, an improved adsorption behavior from 86 to 98% was achieved using MnO_2@EDTA and MnO_2@EDTA-Ag, respectively. Moreover, the initial Cu(II) concentration, which varied between 10 and 50 mg L^{-1} at pH 6.00, had a substantial impact on the adsorption behavior. As shown in Fig. 7 d, when the Cu(II) concentration rose from 10 to 50 mg L^{-1}, the Cu(II) removal efficiency (%) onto MnO_2@EDTA and MnO_2@EDTA-Ag decreased from 86 and 98% to 18% and 33%, respectively. Insufficient active sites on the adsorbent or a lack of equilibrium time for higher concentration adsorption can be ascribed to the decline in the percentage of Cu(II) removal with increasing initial concentration.

Effect of adsorbent dosage

The removal performance (%) of Cu(II) was further investigated using different dosages of adsorbent in the range of 0.5–10 g L^{-1}. The Cu(II) concentration was initially 10 mg L^{-1} and was adjusted for an optimal pH of 6.00 in 90 min. As shown in Fig. 7 e, increasing the dosage of adsorbent from 0.5 to 10 g L^{-1} enhanced the removal efficiency (%)

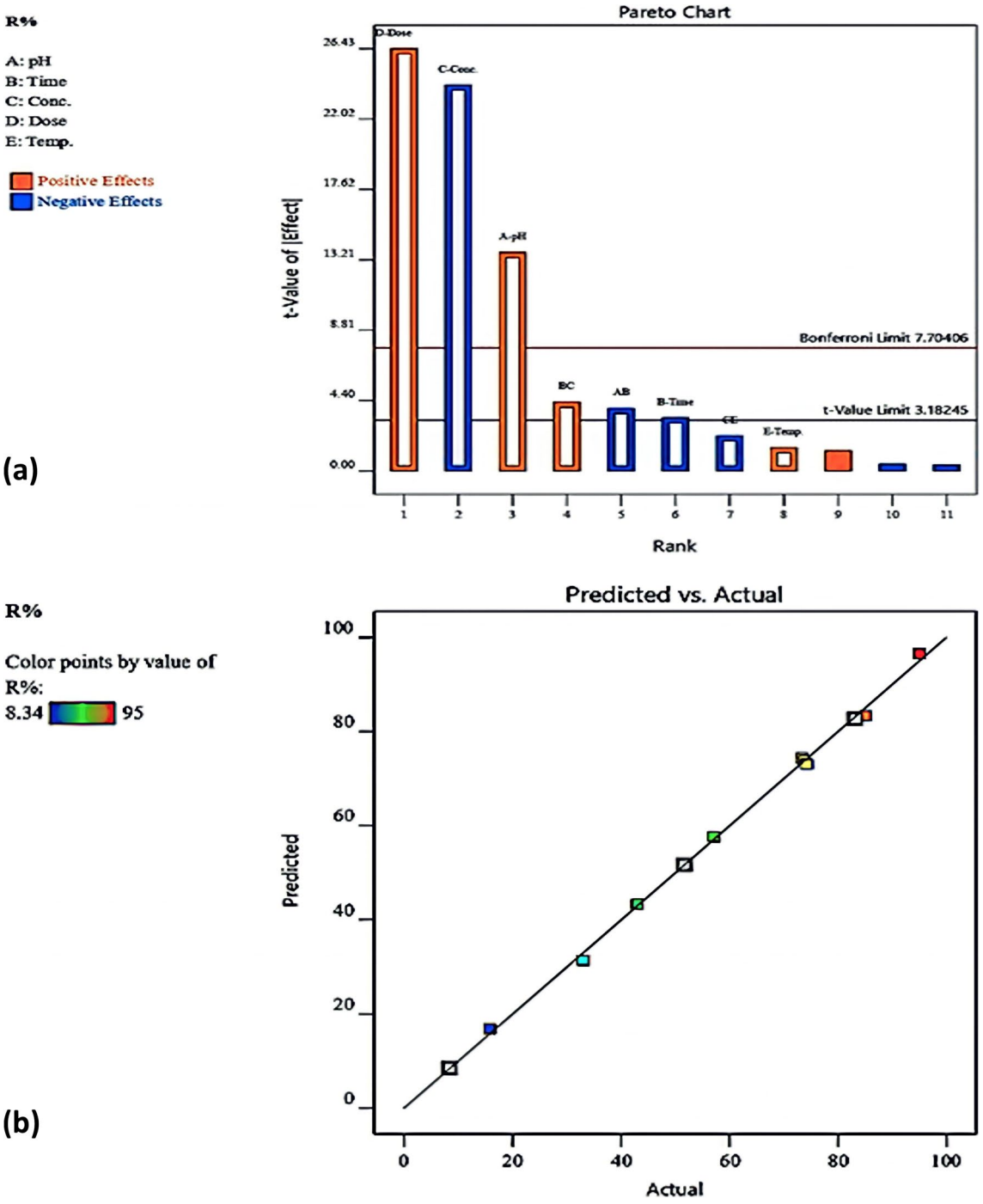

Fig. 5 **a** Pareto chart of the impacts of various parameters on the Cu(II) removal and **b** graphical representation of experimental values as a function of predicted values

of Cu(II) from 30.86 to 95.40% and from 51.9 to 99.8% using MnO_2@EDTA and MnO_2@EDTA-Ag, respectively. The elimination (%) of Cu(II) remained essentially constant as the adsorbent dosage was increased to 10 g L^{-1}. It was evident that the adsorption efficiency considerably increased with elevating the amount of adsorbent due to the higher number of active sites and porous surfaces (Zare et al. 2015).

Effect of ionic strength and interfering ions

Figure 7f presents the effect of ionic strength on the removal (%) of Cu(II) from an aqueous solution. The removal rate (%) dramatically decreased as the NaCl concentration changed, demonstrating the considerable influence of ionic strength on Cu(II) uptake. The effectiveness of Cu(II) adsorption decreased

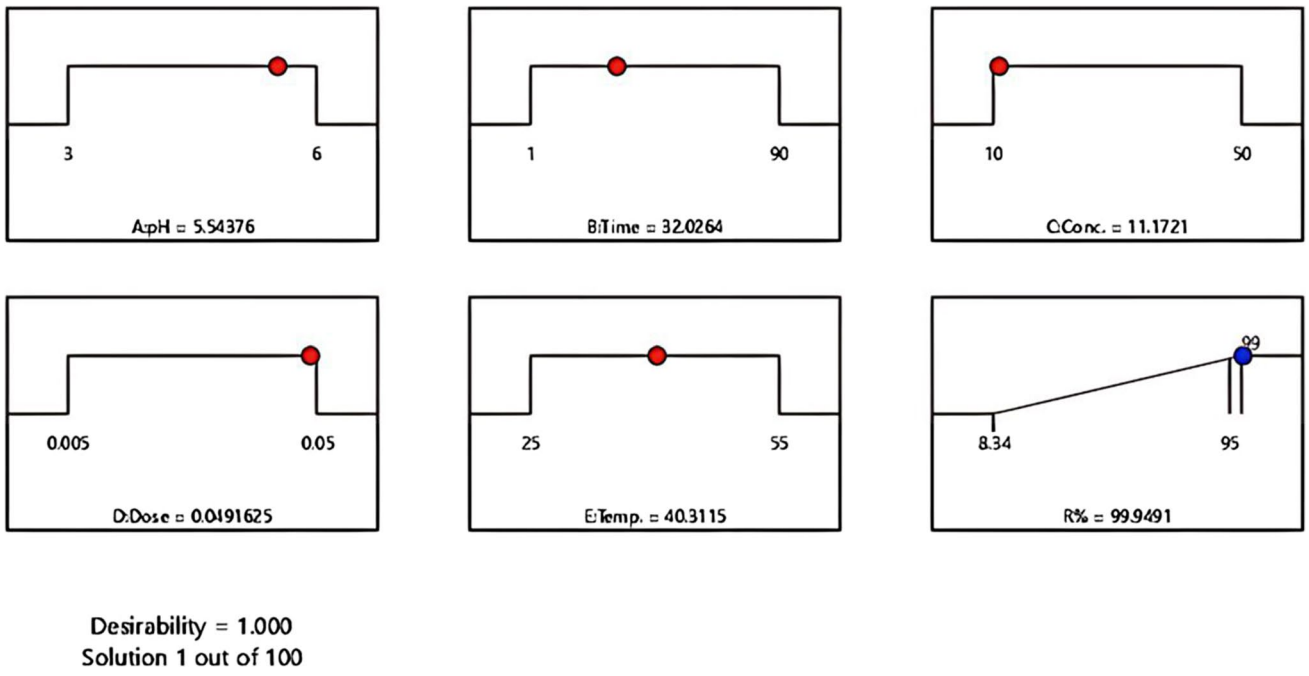

Fig. 6 Predicting points of actual profiles regarding the best settings for copper removal

from 98 to 49% when NaCl concentration increased from 0 to 1.00 mol L^{-1}. This finding can be accounted for by the development of electrostatic screening between the Cu(II) cations and the negative surface of the MnO_2@EDTA-Ag adsorbent (Dinh et al. 2020). Additionally, it was examined how different anions, including Cl^-, NO_3^-, HCO_3^-, SO_4^{2-}, and different cations, such as Na^+, K^+, Mg^{2+}, and Ca^{2+}, affected the removal (%) of Cu(II) by MnO_2@EDTA-Ag. The Cu(II) removal efficiency (%) was not notably affected by the existence of Cl^-, NO_3^-, HCO_3^-, and SO_4^{2-}. Contrarily, Na^+, K^+, Mg^{2+}, and Ca^{2+} significantly hindered Cu(II) adsorption; as a result, the percentage of Cu(II) removed from the sample reduced from 98 to 93, 91, 89, and 85%, respectively. The competition between these cations for adsorption sites on the MnO_2@EDTA-Ag surface was the cause of the observed inhibitory effect.

Kinetic studies

The rate at which Cu(II) ions are removed using the prepared adsorbents from aqueous solutions can be investigated using kinetic studies, which also provide valuable data for identifying the adsorption mechanism. In this regard, several models are employed, including pseudo-first-order, pseudo-second-order, and intra-particle diffusion models. The linearized forms of the employed kinetic models (Sun et al. 2021) are given in Table S1.

The kinetic constants and correlation coefficients (R^2) for the applied models were evaluated (Lima et al. 2019), and their corresponding values are demonstrated in Table 4. Also, RMSE, ΔQ, and χ^2 (Table S2) were employed to assess the consistency of the computational models and experimental points (Khadhri et al. 2019). As demonstrated by the low values of RMSE, ΔQ, and χ^2 and the high values of R^2 (Table 4), pseudo-second-order kinetics (Fig. 8a) rather than pseudo-first-order govern Cu(II) removal onto MnO_2@EDTA and MnO_2@EDTA-Ag. Furthermore, the determined q_e values using the pseudo-second-order model are more consistent with the experimental q_e values, revealing that the pseudo-second-order kinetics effectively describe the Cu(II) removal using MnO_2@EDTA and MnO_2@EDTA-Ag.

Although the pseudo-second-order model provides a sufficiently accurate description of the overall adsorption kinetics, it provides no details on the rate-regulating steps. Therefore, kinetic data were investigated with the Weber and Morris intraparticle diffusion model. To estimate k_i and C values, the intercept and slope of the plot of q_t versus $t^{0.5}$ were utilized. The plots of this model are shown in Fig. 8b, which reveals the occurrence of two stages in the case of Cu(II) removal using MnO_2@EDTA-Ag. The initial stage was the film diffusion attributed to the external mass transfer of Cu(II) ions from the bulk solution to the MnO_2@EDTA-Ag's surface, while the second stage involved the Cu(II) ions' passage through the pores of adsorbents (Ali et al. 2020). However, Cu(II) removal using MnO_2@EDTA comprises three stages, the initial was for film diffusion, while the second was attributed to Cu(II) ions diffusion through MnO_2@EDTA pores, followed by the last stage at which the system has reached equilibrium. The two

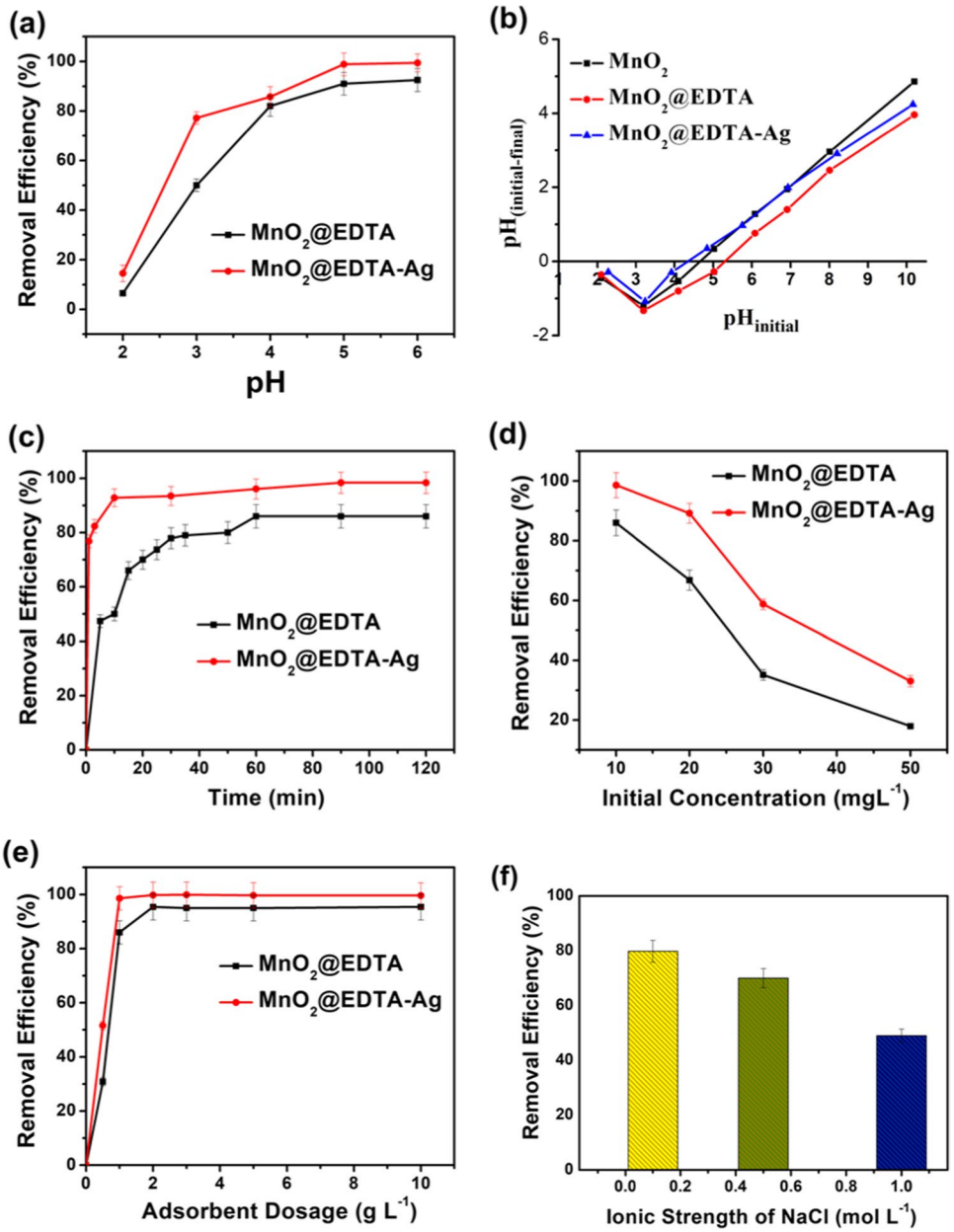

Fig. 7 Effect of **a** initial pH, **b** point of zero charge (pH_{PZC}), **c** time, **d** initial concentration, **e** adsorbent dosage, **f** ionic strength on Cu(II) removal onto MnO_2@EDTA and MnO_2@EDTA-Ag (except **f**, MnO_2@EDTA-Ag only)). ($[Cu^{2+}] = 10$ mg L^{-1} (expect **b**, **d**), [adsorbent dosage] = 1 g L^{-1} (except **e**), pH = 6 (except **a**, **b**), time = 60 min (expect **c**), and temperature = 25 °C)

plots do not cross the origin point, demonstrating that film diffusion in addition to intra-particle diffusion may play a role in the rate-determining stage for controlling Cu(II) removal using MnO_2@EDTA or MnO_2@EDTA-Ag.

Adsorption isotherms

The Cu(II) ions' equilibrium concentrations in the solid and liquid phases were expressed using a variety of models, including the Freundlich, Langmuir, Dubinin–Radushkevich (D-R), and Temkin isotherm models (Mozaffari et al. 2020a; Azzam et al. 2022) These models can be expressed in linearized forms, as demonstrated in Table S3.

The isotherms' constants of the Langmuir and Freundlich models were estimated from their linear plots by plotting C_e/q_e vs. C_e and log q_e vs. log C_e, respectively. Also, plotting ln q_e vs. ε^2 and q_e versus ln C_e enables one to determine the constants K_{DR}, B, and E for the D-R model and the constant b_T for the Temkin model, respectively. Fig. S2 shows the fitting of the experimental data using the applied isotherm models. The calculated parameters of the applied models, along with their R^2, RMSE, ΔQ, and χ^2 values, are summarized in Table 5.

It can be inferred from the high values of R^2 and the low values of RMSE, ΔQ, and χ^2 (Table 5) that the experimental equilibrium results of Cu(II) ions using MnO_2@EDTA or MnO_2@EDTA-Ag are better described by the Langmuir

Table 4 The estimated parameters of the examined kinetic models for Cu(II) removal using MnO_2@EDTA or MnO_2@EDTA-Ag

Kinetic model	Parameters	Adsorbents	
		MnO_2@EDTA	MnO_2@EDTA-Ag
Pseudo-first-order	k_1	0.074	0.067
	$q_{e\ (exp)}$ (mg g^{-1})	8.17	9.35
	$q_{e\ (cal)}$ (mg g^{-1})	7.16	2.19
	R^2	0.9618	0.9083
	RMSE	0.220	0.399
	ΔQ	0.502	0.734
	χ^2	0.410	1.536
Pseudo-second-order	k_2	0.02	0.16
	$q_{e\ (exp)}$ (mg g^{-1})	8.17	9.35
	$q_{e\ (cal)}$ (mg g^{-1})	8.61	9.36
	R^2	0.9991	0.9998
	RMSE	0.121	0.061
	ΔQ	0.046	0.118
	χ^2	0.045	0.014
Intra-particle diffusion	k_i	0.295	0.078
	C	5.75	8.53
	R^2	0.9024	0.9403
	RMSE	0.087	0.055
	ΔQ	0.013	0.007
	χ^2	0.004	0.002

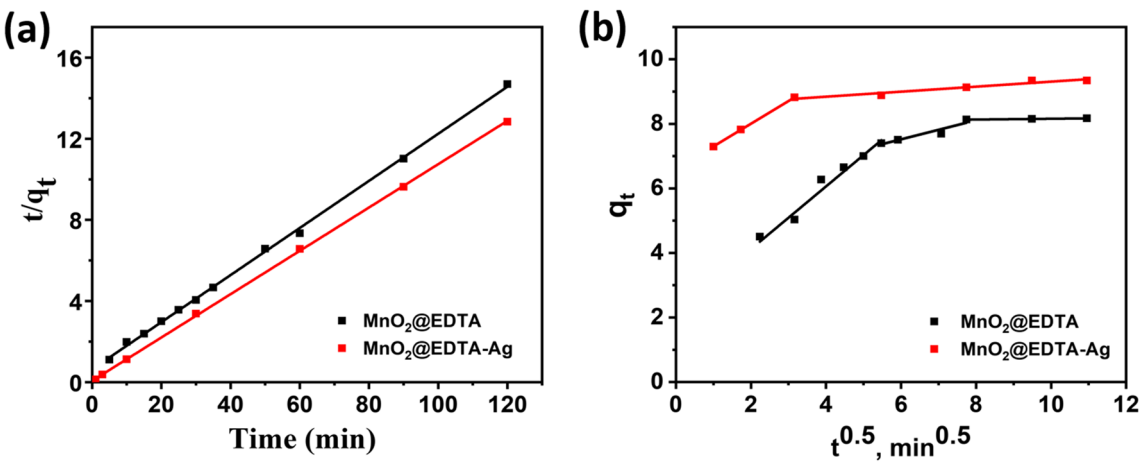

Fig. 8 Plots of the pseudo-second-order kinetics (**a**) and intra-particle diffusion (**b**) for Cu(II) removal onto MnO_2@EDTA and MnO_2@EDTA-Ag

model than the Freundlich model. Also, the R_L values (between 0 and 1) demonstrated favorable adsorption of Cu(II) onto MnO_2@EDTA or MnO_2@EDTA-Ag (Mohamed et al. 2023). Based on the Langmuir isotherm, single-layer adsorption of Cu(II) ions takes place on an even surface of MnO_2@EDTA or MnO_2@EDTA-Ag with a limited number of sites for adsorption. In contrast, the Freundlich model is employed for investigating the interaction of adsorbed molecules on heterogeneous surfaces.

The maximum adsorption capacity (q_{max}) of MnO_2@EDTA-Ag for copper removal was also compared to those of previous studies, as illustrated in Table 6. As concluded, MnO_2@EDTA-Ag can be regarded as an effective adsorbent based on comparison with other adsorbents.

To identify the kind of adsorption—physisorption or chemisorption—the equilibrium data were modeled applying the D-R isotherm. As noticed from Table 5, Cu(II) adsorption onto MnO_2@EDTA and MnO_2@EDTA-Ag was physical in nature because the obtained values of E were < 8 kJ mol^{-1}

Table 5 The estimated parameters of the examined isotherm models for Cu(II) removal

Isotherm model	Parameters	Adsorbents	
		MnO_2@EDTA	MnO_2@EDTA-Ag
Freundlich	K_f (mg g^{-1})	7.90	11.16
	n	28.64	13.63
	R^2	0.8883	0.9899
	RMSE	0.061	0.063
	ΔQ	0.260	1.047
	χ^2	0.023	0.021
Langmuir	K_L (L mg^{-1})	1.32	2.00
	q_{max} (mg g^{-1})	9.24	14.44
	R^2	0.9991	0.9992
	R_L	0.015	0.010
	RMSE	0.046	0.026
	ΔQ	0.142	0.849
	χ^2	0.013	0.018
D-R	B	0.081	0.016
	K_{DR}	8.94	13.71
	E (kJ mol^{-1})	2.480	5.554
	R^2	0.8423	0.9591
	RMSE	0.053	0.170
	ΔQ	0.029	0.086
	χ^2	0.005	0.044
Temkin	b_T (kJ mol^{-1})	8.255	2.863
	R^2	0.8776	0.9942
	RMSE	0.129	0.132
	ΔQ	0.017	0.012
	χ^2	0.008	0.005

(Kakavandi et al. 2015). Moreover, the Temkin constant (b_T) has been determined to provide further details on the physical nature of Cu(II) adsorption onto the prepared adsorbents. It was found that the values of b_T were 8.255 and 2.863 kJ mol^{-1} for MnO_2@EDTA and MnO_2@EDTA-Ag, respectively, revealing weak electrostatic interactions (Mohammadnezhad et al. 2017).

Thermodynamic studies

At various temperatures (298–328 K), the sorption process' thermodynamic characteristics were assessed. The following equations were used to estimate the enthalpy change (ΔH, kJ mol^{-1}), entropy change (ΔS, J mol^{-1} K^{-1}), and free energy change (ΔG, kJ mol^{-1}) (Ali and Mohamed 2017):

$$K_d = \frac{q_e}{C_e} \tag{5}$$

$$\Delta G = -\mathrm{RT}\ \mathrm{In}\ K_d \tag{6}$$

$$\ln\ K_d = \frac{\Delta S}{R} - \frac{\Delta H}{\mathrm{RT}} \tag{7}$$

where R is the universal gas constant (8.314 J K^{-1} mol^{-1}), T is the temperature in Kelvin, and K_d is the equilibrium constant. The slope and intercept of the plot of ln K_d vs 1/T can be used to determine the values of ΔH and ΔS.

As shown in Table 7, for the adsorption of Cu(II) onto MnO_2@EDTA and MnO_2@EDTA-Ag, the positive and negative values of ΔH revealed that the nature of the adsorption process was endothermic and exothermic, respectively. When the value of ΔH is less than 80 kJ mol^{-1}, the adsorption process involves physisorption, such as van der Waals or electrostatic interaction, and when the value of ΔH is greater than 80 kJ mol^{-1}, the interaction is chemisorption (Ali and Mohamed 2017).

Table 6 Comparison of the adsorption capacity of MnO_2@EDTA-Ag nanocoral reef with other adsorbents

Adsorbent	Cu(II) uptake (mg g^{-1})	References
Spent-grain	10.47	Lu and Gibb (2008)
Powdered banana peel waste	3.29	Seleman et al. (2023)
Chitosan/ZnO nanorod composite	8.01	Ali and Mohamed (2017)
Rubber leaves powder	9.07	Rukayat et al. (2021)
Alg/MWCNTs/DAC nanocomposite	26.6	Eldeeb et al. (2021)
PMMA/SilicaKit6	9.03	Dinari et al. (2016)
Coated chitosan on alumina	86.2	Boddu et al. (2008)
Ni ferrite-modified montmorillonite	18.73	Ahmed et al. (2021)
Carbon gel doped with graphite	8.64	Osińska (2017)
CS-SiO_2@TEuTTA membrane	51.28	Li et al. (2023)
PBAT microplastics	0.192	Sun et al. (2023)
ALG-HT biocomposite	63.25	Menye et al. (2023)
CuO-modified ceramic membrane	13.03	Mahatmanti et al. (2023)
MnO_2@EDTA-Ag	14.44	This work

Table 7 Thermodynamic parameters for Cu(II) removal using MnO_2@EDTA and MnO_2@EDTA-Ag adsorbents

Adsorbent	ΔH (kJ mol^{-1})	ΔS (J mol^{-1} K^{-1})	ΔG (kJ mol^{-1})			
			298 K	308 K	318 K	328 K
MnO_2@EDTA	33.56	107.25	1.482	0.409	− 0.662	− 1.735
MnO_2@EDTA-Ag	− 38.73	− 128.82	− 0.349	0.938	2.226	3.514

The adsorption was favorable since the positive values for ΔS suggested a rise in randomness at the solid-solution interface. The disorder at the solid/liquid boundary (interface) was reduced throughout the adsorption process of the copper ions, as shown by the negative value of ΔS (− 128.82 J K^{-1} mol^{-1}) obtained using MnO_2@EDTA-Ag. Because copper ions are more mobile at higher temperatures, ions from the solid phase were able to move into the liquid phase. Therefore, less amount of copper could be adsorbed (Rukayat and Usman 2021). The negative ΔG values at the higher temperatures demonstrated the viability and spontaneity of the Cu(II) sorption process onto MnO_2@EDTA, whereas the positive ΔG values at the lower temperatures reflected the non-spontaneous character of the adsorption process. On the contrary, Cu(II) adsorption onto MnO_2@EDTA-Ag was spontaneous at the lower temperatures and non-spontaneous at the higher ones.

Desorption and reusability study

To evaluate the desorption behavior of MnO_2@EDTA-Ag, different concentrations of strong acids, such as HCl, H_2SO_4, and HNO_3, ranging from 0.001 to 0.005 mol L^{-1} are most commonly used to elute Cu(II). It was observed that increased concentration of strong acids (0.001–0.005 mol L^{-1}) enhanced the desorption efficiency (%) of Cu(II) from 30.24 to 77.55%, 35.66 to 82.16%, and 77.50 to 92% using HCl, H_2SO_4, and HNO_3, respectively (Fig. 9a). For economic reasons and environmental points of view, recycling of adsorbents has a significant role. Herein, 0.005 mol L^{-1} HNO_3 was used as a stripping agent for regeneration of MnO_2@EDTA-Ag. After the adsorption process of Cu(II), MnO_2@EDTA-Ag was recollected and mixed with 10 mL HNO_3 (0.005 mol L^{-1}), shaken for 1 h, and separated. The collected adsorbent was washed with distilled water and dried to be reused again. The Cu(II) solution was added again to the collected adsorbent to evaluate the stability of the adsorbent. After completing three consecutive cycles of

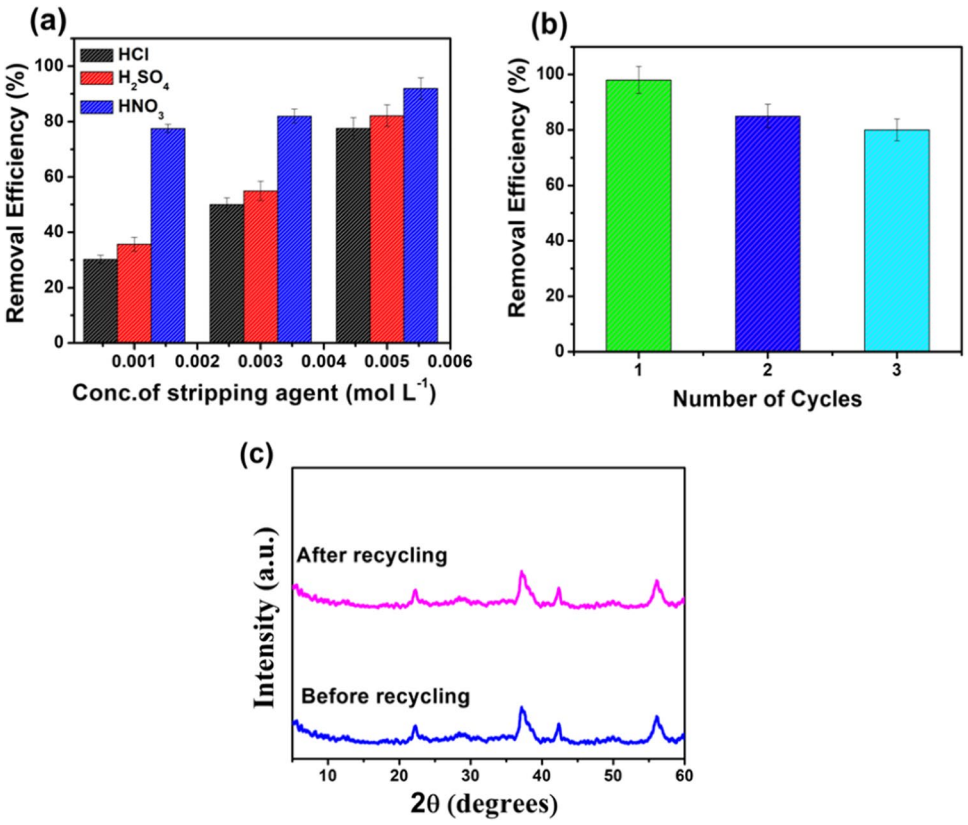

Fig. 9 **a** Effect of stripping agents for desorption study, **b** recycling of MnO_2@EDTA-Ag for Cu(II) removal, and **c** XRD patterns of MnO_2@EDTA-Ag before and after the third cycle

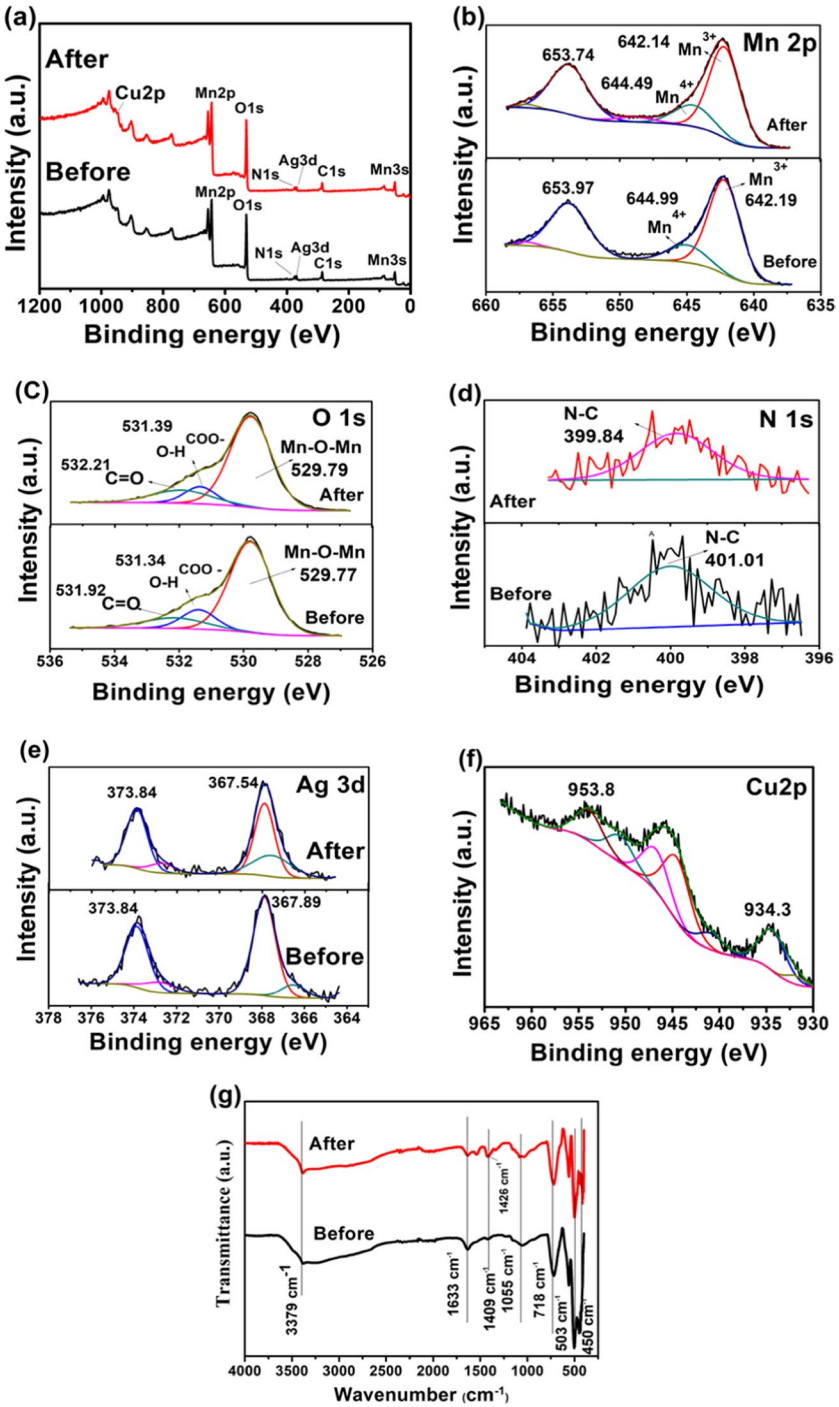

Fig. 10 XPS and FTIR analysis before and after adsorption of Cu(II) onto MnO_2@EDTA-Ag: **a** full survey, **b** Mn 2p, **c** O 1s, **d** N 1s, **e** Ag 3d, **f** Cu 2p, and **g** FTIR spectra

adsorption–desorption, the efficacy of MnO_2@EDTA-Ag for removing Cu(II) was slightly reduced, as shown in Fig. 9b. The removal efficiency % of the Cu(II) solution was reduced from 98 to 80%. In addition, there is no significant change in the XRD analysis before and after the recycling process, implying its stability (Fig. 9c). The results demonstrated that the MnO_2@EDTA-Ag nanocoral reef was comparably stable under the studied conditions, which is an advantage of using the adsorbent for environmental remediation and the industrial field.

Proposed removal mechanism of Cu(II) onto MnO_2@EDTA-Ag

The adsorption mechanism has been comprehensively elucidated using XPS and FTIR analysis. The chemical states of MnO_2@EDTA-Ag nanocoral reef before and after Cu(II) adsorption were investigated by XPS analysis. Figure 10a illustrates the XPS survey spectra of both samples before and after Cu(II) removal, where the typical Mn, Ag, C, O, and N signals

could be observed. Meanwhile, the newly appeared peak of the Cu(II) signal could be found in the sample after adsorption, confirming the uptake of Cu(II) ions onto the MnO_2@EDTA-Ag nanocoral reef. The high-resolution scan of the Mn 2p spectrum is given in Fig. 10b. The peaks located around binding energies of 642.14 and 653.74 eV are assigned to Mn $2p_{3/2}$ and Mn $2p_{1/2}$. The Mn $2p_{3/2}$ and Mn $2p_{1/2}$ peaks showed a splitting of 11.55 eV, which confirms that the main oxidation state of Mn atoms is+4. The values of binding energy at 642.19 and 644.99 eV of the Mn $2p_{3/2}$ spectrum are ascribed to Mn^{3+} and Mn^{4+}, respectively. After Cu(II) adsorption, the binding energy of the Mn $2p_{3/2}$ spectrum is slightly shifted to 642.14 and 644.49 eV, confirming the absence of Mn^{2+} in the MnO_2@EDTA-Ag nanocoral reef. In addition, the Mn^{3+}/Mn^{4+} ratio of MnO_2@EDTA-Ag nanocoral reef is slightly increased from 3.40 to 4.38% after the adsorption process, confirming the absence of redox reactions (Lin and Chen 2020). As shown in Fig. 10c, the O 1 s spectrum before and after adsorption was elucidated. The peak located at 529.77 eV is attributed to lattice oxygen of metal oxide (Mn–O–Mn bonds), the peak at 531.34 eV corresponds to Mn–OH and $–COO^-$ groups, and the peak at higher binding energy, 531.92 eV, associated with OH groups of water molecules or carbonyl groups (Claros et al. 2021). After adsorption of Cu(II) to the surface of MnO_2@EDTA-Ag, the peaks of 531.34 and 531.92 eV are shifted to 531.39 and 532.12 eV, respectively. The relative area ratio for the peak of the Mn–O bond is slightly increased from 74.21 to 74.24% due to the binding of Mn–O, Cu–O, and the formation of bidentate mononuclear or multidentate complexes, instead of monodentate complexes during the adsorption. Meanwhile, the relative ratio of Mn–OH decreased from 13.06 to 10.58% due to the participation of the hydroxyl groups in the adsorption process (Lin and Chen 2020; Claros et al. 2021). Before the adsorption of Cu(II), the value of binding energy of N 1s spectrum (Fig. 10d) was 401.01 eV, which is slightly shifted to 399.84 eV after the adsorption process, suggesting that Cu(II) ions may be bound to N atoms of EDTA by chelation interaction (Cui et al. 2021). Therefore, the synergistic effect between the physisorption forces and the chelation interaction of MnO_2@EDTA-Ag nanocoral reef enhanced Cu(II) removal. The Ag 3d spectrum (Fig. 10e) before and after Cu(II) adsorption exhibits only a couple of peaks at binding energies of 367.89 and 373.84 eV, corresponding to Ag $3d_{5/2}$ and $Ag3d_{3/2}$, respectively, showing the presence of metallic Ag (NPs) (Bai et al. 2016; Tang et al. 2019). The relative area ratio of Ag $3d_{5/2}$ decreased from 52.91% (before adsorption) to 38.52% (after adsorption). This decrease may be due to the adsorption of Cu(II) onto MnO_2@EDTA-Ag. The binding energies at 934.3 and 953.8 eV (Fig. 10f) are attributed to Cu $2p_{3/2}$ and Cu $2p_{1/2}$, with a spin–orbit separation of 19.5 eV, implying the removal of Cu(II) ions onto MnO_2@EDTA-Ag nanocoral reef (Claros et al. 2021). In addition, the "shake-up" satellite peaks in the range 940–945 eV are evidence for the presence of Cu^{2+} state (Mulla and Rabinal 2021).

Additionally, Fig. 10g displays the MnO_2@EDTA-Ag FTIR spectra before and after Cu(II) capture. Following Cu(II) adsorption, the peak at 1409 cm^{-1} ascribed to the symmetric stretching vibration of C–N bonds and COO^- groups that originated from EDTA shifted to 1426 cm^{-1}. This implies that these groups participate in the formation of a coordination complex involving Cu(II).

Environmental applications

The analytical usefulness of MnO_2@EDTA-Ag to be employed for water remediation was demonstrated by applying them to remove Cu(II) ions that were spiked in different water samples, including groundwater, Nile water, and tap water. This was carried out by shaking 0.01 g of MnO_2@EDTA-Ag for 1 h, at pH 6 with 10 mL of each water sample that was previously spiked with 10 mg mL^{-1} Cu(II). The results are presented in Fig. S3, which revealed no significant difference in the removal efficiency of MnO_2@EDTA-Ag in any of the water samples tested, reflecting the effectiveness of the prepared samples in wastewater treatment. It is worth mentioning that the equilibrium Cu(II) concentration in all the tested samples was all less than 0.7 mg L^{-1}, demonstrating the remarkable effectiveness of MnO_2@EDTA-Ag to remediate complex wastewater from heavy metals.

Conclusion

In this work, a novel MnO_2@EDTA-Ag nanocoral reef was effectively synthesized via a facile redox reaction followed by impregnation with EDTA and silver nanoparticles for rapid removal of hazardous copper (II) from real water samples. The results showed that the nanocoral reef structure's Cu(II) removal efficiency (99.95%) employing Plackett–Burman design (PBD) was achieved at pH 5.5, a contact time of 32.0 min, a Cu(II) concentration of 11.2 mg L^{-1}, MnO_2@EDTA-Ag dose of 0.05 g, and a temperature of 40.3 °C. The proposed model with PBD revealed that the dose of MnO_2@EDTA-Ag, followed by Cu(II) concentration and pH, were the most significant parameters affecting Cu(II) removal. It was found that the loading of Ag NPs onto MnO_2@EDTA improved the adsorption capability of MnO_2@EDTA-Ag. The adsorption data were significantly correlated with the models of pseudo-second-order kinetics and Langmuir isotherm. Moreover, the thermodynamic study of the Cu(II) removal is energetically exothermic. XPS and FTIR analysis elucidated that the electrostatic interaction and chelation/complexation are responsible for the removal mechanisms of Cu(II). No significant loss in the Cu(II) removal efficiency using the real wastewater samples compared to the aqueous solution was observed, revealing its efficacy in water remediation. Additionally,

the recyclability of MnO_2@EDTA-Ag nanocoral reef for Cu(II) was maintained at 80% after three adsorption–desorption cycles, and the XRD data before and after the recycling process revealed no significant changes, suggesting its stability. According to these conclusions, the MnO_2@EDTA-Ag nanocoral reef shows promise as a sorbent for the removal of potentially hazardous metals from wastewater.

Supplementary Information The online version contains supplementary material available at https://doi.org/10.1007/s11356-023-30805-0.

Acknowledgements The authors would like to thank the Faculty of Science at Helwan University for allowing them to use the faculty's resources for this study. In addition, the authors are grateful to the National Research Centre for providing equipment facilities.

Author contribution All persons who meet authorship criteria are listed as authors, and all authors certify that they have participated sufficiently in the work to take public responsibility for the content, including participation in the concept, design, analysis, writing, or revision of the manuscript. Furthermore, each author certifies that this material or similar material has not been and will not be submitted to or published in any other publication before its appearance in the *Environmental Science and Pollution Research.*

Category 1

Conception and design of study: Omnia I. Ali, Ahmed B. Azzam

Acquisition of data: Omnia I. Ali, Ahmed B. Azzam

Analysis and/or interpretation of data: Omnia I. Ali, Ahmed B. Azzam

Category 2

Drafting the manuscript: Omnia I. Ali, Ahmed B. Azzam

Revising the manuscript critically for important intellectual content: Omnia I. Ali, Ahmed B. Azzam

Category 3

Approval of the version of the manuscript to be published: Omnia I. Ali, Ahmed B. Azzam

Funding Open access funding provided by The Science, Technology & Innovation Funding Authority (STDF) in cooperation with The Egyptian Knowledge Bank (EKB).

Data availability Raw data is available upon request.

Declarations

Ethics approval This work does not contain any investigations with human participants or animals performed by any of the authors.

Consent to participate Not applicable.

Consent to publish Not applicable.

Competing interests The authors declare no competing interests.

References

Ahmed HA, Soliman MSS, Othman SA (2021) Synthesis and characterization of magnetic nickel ferrite-modified montmorillonite nanocomposite for Cu (II) and Zn (II) ions removal from wastewater. Egypt J Chem 64:5627–5645. https://doi.org/10.21608/ejchem.2021.69597.3527

Ali O, Mohamed S (2017) Adsorption of copper ions and alizarin red S from aqueous solutions onto a polymeric nanocomposite in single and binary systems. Turkish J Chem 41:967–986. https://doi.org/10.3906/kim-1703-72

Ali OIM, El Menofy EA, Kandil AHHT (2020) Synthesis, characterisation and application of ZnO-bentonite nanocomposite for preconcentration and spectrophotometric determination of trace amounts of bromocresol purple in water and wastewater samples. Int J Environ Anal Chem 100:746–763. https://doi.org/10.1080/03067319.2019.1639689

Al-Saydeh SA, El-Naas MH, Zaidi SJ (2017) Copper removal from industrial wastewater: a comprehensive review. J Ind Eng Chem 56:35–44. https://doi.org/10.1016/j.jiec.2017.07.026

Asim U, Husnain SM, Abbas N et al (2021) Morphology controlled facile synthesis of MnO2 adsorbents for rapid strontium removal. J Ind Eng Chem 98:375–382. https://doi.org/10.1016/j.jiec.2021.03.027

Azzam AB, Tokhy YA, El Dars FM, Younes AA (2022) Construction of porous biochar decorated with NiS for the removal of ciprofloxacin antibiotic from pharmaceutical wastewaters. J Water Process Eng 49:103006. https://doi.org/10.1016/j.jwpe.2022.103006

Bai B, Qiao Q, Arandiyan H et al (2016) Three-dimensional ordered mesoporous MnO2 -supported Ag nanoparticles for catalytic removal of formaldehyde. Environ Sci Technol 50:2635–2640. https://doi.org/10.1021/acs.est.5b03342

Bakatula EN, Richard D, Neculita CM, Zagury GJ (2018) Determination of point of zero charge of natural organic materials. Environ Sci Pollut Res 25:7823–7833. https://doi.org/10.1007/s11356-017-1115-7

Bigiani L, Zappa D, Maccato C et al (2020) Quasi-1D MnO2 nanocomposites as gas sensors for hazardous chemicals. Appl Surf Sci 512:145667. https://doi.org/10.1016/J.APSUSC.2020.145667

Boddu VM, Abburi K, Randolph AJ, Smith ED (2008) Removal of copper (II) and nickel (II) ions from aqueous solutions by a composite chitosan biosorbent. Sep Sci Technol 43:1365–1381. https://doi.org/10.1080/01496390801940762

Cao R, Li L, Zhang P (2021) Macroporous MnO2-based aerogel crosslinked with cellulose nanofibers for efficient ozone removal under humid condition. J Hazard Mater 407:124793. https://doi.org/10.1016/j.jhazmat.2020.124793

Chen S, Xie F (2020) Selective adsorption of Copper (II) ions in mixed solution by Fe3O4-MnO2-EDTA magnetic nanoparticles. Appl Surf Sci 507:145090. https://doi.org/10.1016/j.apsusc.2019.145090

Choudhary M, Kumar R, Neogi S (2020) Activated biochar derived from Opuntia ficus-indica for the efficient adsorption of malachite green dye, Cu+2 and Ni+2 from water. J Hazard Mater 392:122441. https://doi.org/10.1016/j.jhazmat.2020.122441

Claros M, Kuta J, El-Dahshan O et al (2021) Hydrothermally synthesized MnO2 nanowires and their application in Lead (II) and Copper (II) batch adsorption. J Mol Liq 325:115203. https://doi.org/10.1016/j.molliq.2020.115203

Cui C, Sun X, Zhou C et al (2021) Pomegranate-like MnO2@PANI sub-microspheres: synthesis and application for Pb(II) ions removal from water. Colloids Surf A Physicochem Eng Asp 616:126336. https://doi.org/10.1016/j.colsurfa.2021.126336

Dastkhoon M, Ghaedi M, Asfaram A, Javadian H (2018) Synthesis of CuS nanoparticles loaded on activated carbon composite for ultrasound-assisted adsorption removal of dye pollutants: process optimization using CCD-RSM, equilibrium and kinetic studies. Appl Organomet Chem 32:1–11. https://doi.org/10.1002/aoc.4350

Devaraj S, Munichandraiah N (2008) Effect of crystallographic structure of MnO2 on its electrochemical capacitance properties. J Phys Chem C 112:4406–4417. https://doi.org/10.1021/jp7108785

Dinari M, Mohammadnezhad G, Soltani R (2016) Fabrication of poly(methyl methacrylate)/silica KIT-6 nanocomposites via in situ polymerization approach and their application for removal of Cu2+ from aqueous solution. RSC Adv 6:11419–11429. https://doi.org/10.1039/C5RA23500F

Dinh VP, Nguyen MD, Nguyen QH et al (2020) Chitosan-MnO2 nanocomposite for effective removal of Cr (VI) from aqueous solution. Chemosphere 257:127147. https://doi.org/10.1016/j.chemosphere.2020.127147

Duan G, Li X, Ma X et al (2023) High-efficiency adsorption removal for Cu(II) and Ni(II) using a novel acylamino dihydroxamic acid chelating resin. Sci Total Environ 864:160984. https://doi.org/10.1016/j.scitotenv.2022.160984

Eldeeb TM, El-nemr A, Khedr MH, El-dek SI (2021) Novel bionanocomposite for efficient copper removal. Egypt J Aquat Res 47:261–267. https://doi.org/10.1016/j.ejar.2021.07.002

Elfiad A, Galli F, Boukhobza LM et al (2020) Low-cost synthesis of Cu/α-Fe2O3 from natural HFeO2: application in 4-nitrophenol reduction. J Environ Chem Eng 8:104214. https://doi.org/10.1016/j.jece.2020.104214

El-naggar NE, Hamouda RA, Mousa IE, Abdel-hamid MS (2018) Statistical optimization for cadmium removal using Ulva fasciata biomass : characterization, immobilization and application for almost-complete cadmium removal from aqueous solutions. Sci Rep 8:12456. https://doi.org/10.1038/s41598-018-30855-2

Fu Y, Xu P, Huang D et al (2019) Au nanoparticles decorated on activated coke via a facile preparation for e ffi cient catalytic reduction of nitrophenols and azo dyes. Appl Surf Sci 473:578–588. https://doi.org/10.1016/j.apsusc.2018.12.207

Ghosh SK (2020) Diversity in the family of manganese oxides at the nanoscale: from fundamentals to applications. ACS Omega 5:25493–25504. https://doi.org/10.1021/acsomega.0c03455

Guo J, Gao Q, Chen Y et al (2021) Insight into sludge dewatering by advanced oxidation using persulfate as oxidant and Fe2+ as activator: performance, mechanism and extracellular polymers and heavy metals behaviors. J Environ Manag 288:112476. https://doi.org/10.1016/j.jenvman.2021.112476

Hama Aziz KH, Mustafa FS, Omer KM et al (2023) Heavy metal pollution in the aquatic environment: efficient and low-cost removal approaches to eliminate their toxicity: a review. RSC Adv 13:17595–17610. https://doi.org/10.1039/D3RA00723E

Hao J, Meng X, Fang S et al (2020) MnO2-functionalized amorphous carbon sorbents from spent lithium-ion batteries for highly efficient removal of cadmium from aqueous solutions. Ind Eng Chem Res 59:10210–10220. https://doi.org/10.1021/acs.iecr.9b06670

Hasanpour M, Hatami M (2020) Application of three dimensional porous aerogels as adsorbent for removal of heavy metal ions from water/wastewater: a review study. Adv Colloid Interface Sci 284:102247. https://doi.org/10.1016/j.cis.2020.102247

Husnain SM, Asim U, Yaqub A et al (2020) Recent trends of MnO2-derived adsorbents for water treatment: a review. New J Chem 44:6096–6120. https://doi.org/10.1039/c9nj06392g

Kakavandi B, Kalantary RR, Jafari AJ et al (2015) Pb(II) Adsorption onto a magnetic composite of activated carbon and superparamagnetic Fe3O4 nanoparticles: experimental and modeling study. Clean - Soil, Air, Water 43:1157–1166. https://doi.org/10.1002/clen.201400568

Khadhri N, El Khames Saad M, Ben Mosbah M, Moussaoui Y (2019) Batch and continuous column adsorption of indigo carmine onto activated carbon derived from date palm petiole. J Environ Chem Eng 7:102775. https://doi.org/10.1016/j.jece.2018.11.020

Kuang Y, Zhang Z, Wu D (2022) Synthesis of graphene oxide/polyethyleneimine sponge and its performance in the sustainable removal of Cu(II) from water. Sci Total Environ 806:151258. https://doi.org/10.1016/j.scitotenv.2021.151258

Lee MY, Wang WL, Du Y et al (2021) Applications of UV/H2O2, UV/persulfate, and UV/persulfate/Cu2+ for the elimination of reverse osmosis concentrate generated from municipal wastewater reclamation treatment plant: toxicity, transformation products, and disinfection byproducts. Sci Total Environ 762:144161. https://doi.org/10.1016/j.scitotenv.2020.144161

Li L, Xi P, Wang X, Cheng B (2023) Luminescent CS-SiO2@TEuTTA membrane for simultaneous detection and adsorption of copper(II) ions. J Environ Chem Eng 11. https://doi.org/10.1016/j.jece.2023.109573

Lima DR, Lima EC, Umpierres CS et al (2019) Removal of amoxicillin from simulated hospital effluents by adsorption using activated carbons prepared from capsules of cashew of Para. Environ Sci Pollut Res 26:16396–16408. https://doi.org/10.1007/s11356-019-04994-6

Lin M, Chen Z (2020) A facile one-step synthesized epsilon-MnO2 nanoflowers for effective removal of lead ions from wastewater. Chemosphere 250:126329. https://doi.org/10.1016/j.chemosphere.2020.126329

Liu S, Ji J, Yu Y, Huang H (2018) Catalysis Science & Technology Facile synthesis of amorphous mesoporous decomposition of ozone. 4264–4273. https://doi.org/10.1039/c8cy01111g

Lu S, Gibb SW (2008) Copper removal from wastewater using spent-grain as biosorbent. Bioresour Technol 99:1509–1517. https://doi.org/10.1016/j.biortech.2007.04.024

Mahatmanti FW, Jumaeri J, Kusumastuti E (2023) The adsorption behavior of individual Cu(II), Zn(II), and Cd(II) ions over a CuO-modified ceramic membrane synthesized from fly ash. J King Saud Univ - Sci 35:102866. https://doi.org/10.1016/j.jksus.2023.102866

Mallakpour S, Motirasoul F (2017) Use of PVA/α-MnO2-stearic acid nanocomposite films prepared by sonochemical method as a potential sorbent for adsorption of Cd (II) ion from aqueous solution. Ultrason Sonochem 37:623–633. https://doi.org/10.1016/j.ultsonch.2017.02.025

Markovski JS, Marković DD, Dokić VR et al (2014) Arsenate adsorption on waste eggshell modified by goethite, α-MnO2 and goethite/α-MnO2. Chem Eng J 237:430–442. https://doi.org/10.1016/j.cej.2013.10.031

Menye S, Tcheka C, Akpomie KG et al (2023) Alginate/Hyphaene thebaica fruit shell biocomposite as environmentally friendly and low-cost biosorbent for heavy metals uptake from aqueous solution: batch equilibrium and kinetic studies. Chem Africa 6:175–190. https://doi.org/10.1007/s42250-022-00514-1

Mohamed TK, Mubarak MF, Keshawy M et al (2023) Ecofriendly maghemite/halloysite-like nanotubes nanocomposite for highly efficient removal of Cd(II) from industrial wastewater. Arab J Sci Eng 48:7781–7795. https://doi.org/10.1007/s13369-023-07809-6

Mohammadnezhad G, Soltani R, Abad S, Dinari M (2017) A novel porous nanocomposite of aminated silica MCM-41 and nylon-6: isotherm, kinetic, and thermodynamic studies on adsorption of Cu(II) and Cd(II). J Appl Polym Sci 134:45383. https://doi.org/10.1002/app.45383

Mozaffari N, Mirzahosseiniv AHS, Mozaffari N (2020a) A new kinetic models analysis for CO adsorption on palladium zeolite nanostructure by roll-coating technique. Anal Methods Environ Chem J 3:92–107. https://doi.org/10.24200/amecj.v3.i02.106

Mozaffari N, Mozaffari N, Elahi SM et al (2020b) Kinetics study of CO molecules adsorption on Al2O3/zeolite composite films prepared by roll- coating method. Surf Eng 0:1–10. https://doi.org/10.1080/02670844.2020.1768628

Mozaffari N, Solaymani S, Achour A et al (2020c) New insights into SnO2/Al2O3, Ni/Al2O3, and SnO2/Ni/Al2O3 composite films for CO adsorption: building a bridge between microstructures and adsorption properties. J Phys Chem C 124:3692–3701. https://doi.org/10.1021/acs.jpcc.9b11148

Mulla R, Rabinal MK (2021) CuO/CuxS composites fabrication and their thermoelectric properties. Mater Renew Sustain Energy 10:3. https://doi.org/10.1007/s40243-021-00189-7

Osińska M (2017) Removal of lead(II), copper(II), cobalt(II) and nickel(II) ions from aqueous solutions using carbon gels. J Sol-Gel Sci Technol 81:678–692. https://doi.org/10.1007/s10971-016-4256-0

Panahandeh A, Parvareh A, Moraveji MK (2021) Synthesis and characterization of γ-MnO2/chitosan/Fe3O4 cross-linked with EDTA and the study of its efficiency for the elimination of zinc(II) and lead(II) from wastewater. Environ Sci Pollut Res 28:9235–9254. https://doi.org/10.1007/s11356-020-11359-x

Raheem ZH, Al Sammarraie AMA (2020) Synthesis of different manganese dioxide nanostructures and studding the enhancement of their electrochemical behavior in zinc – MnO2 rechargeable batteries by doping with copper. In: AIP Conf Proc 2213:020187. https://doi.org/10.1063/5.0000246

Repo E, Warchol JK, Kurniawan TA, Sillanpää MET (2010) Adsorption of Co(II) and Ni(II) by EDTA- and/or DTPA-modified chitosan: kinetic and equilibrium modeling. Chem Eng J 161:73–82. https://doi.org/10.1016/j.cej.2010.04.030

Revathi C, Kumar RTR (2017) Electro catalytic properties of α, β, γ, ϵ - MnO2 and γ - MnOOH nanoparticles: role of polymorphs on enzyme free H2O2 sensing. Electroanalysis 29:1481–1489. https://doi.org/10.1002/elan.201600608

Rukayat OO, Usman MF (2021) Adsorption of heavy metal (copper) on rubber (Hevea Brasiliensis) leaf powder. South African J Chem Eng 37:74–80. https://doi.org/10.1016/j.sajce.2021.04.004

Rukayat OO, Usman MF, Elizabeth OM et al (2021) Kinetic adsorption of heavy metal (copper) on rubber (Hevea Brasiliensis) leaf powder. South African J Chem Eng 37:74–80. https://doi.org/10.1016/j.sajce.2021.04.004

Seleman M, Sime T, Ayele A et al (2023) Isotherms and kinetic studies of copper removal from textile wastewater and aqueous solution using powdered banana peel waste as an adsorbent in batch adsorption systems. Int J Biomater 2023:2012069. https://doi.org/10.1155/2023/2012069

Sharif HMA, Mahmood A, Cheng HY et al (2019) Fe3O4 nanoparticles coated with EDTA and Ag nanoparticles for the catalytic reduction of organic dyes from wastewater. ACS Appl Nano Mater 2:5310–5319. https://doi.org/10.1021/acsanm.9b01250

Shi S, Xu C, Dong Q et al (2021) High saturation magnetization MnO2/PDA/Fe3O4 fibers for efficient Pb(II) adsorption and rapid magnetic separation. Appl Surf Sci 541:148379. https://doi.org/10.1016/j.apsusc.2020.148379

Song Q, Wang H, Yang B et al (2016) A novel adsorbent of Ag-FMWCNTs for the removal of SMX from aqueous solution. RSC Adv 6:75855–75861. https://doi.org/10.1039/c6ra15206f

Sun C, Mu Y, Wang Y (2020) A Pd/MnO2 electrocatalyst for nitrogen reduction to ammonia under ambient conditions. Catalysts 10:802. https://doi.org/10.3390/catal10070802

Sun L, Xu K, Gui X et al (2021) Reduction–responsive sulfur–monoterpene polysulfides in microfiber for adsorption of aqueous heavy metal. J Water Process Eng 43:102247. https://doi.org/10.1016/j.jwpe.2021.102247

Sun Y, Peng B-Y, Wang Y et al (2023) Evaluating the adsorption and desorption performance of poly(butylene adipate-co-terephthalate) (PBAT) microplastics towards Cu(II): The roles of biofilms and biodegradation. Chem Eng J 464:142714. https://doi.org/10.1016/j.cej.2023.142714

Tang Z, Yeo BC, Han SS et al (2019) Facile aqueous-phase synthesis of Ag–Cu–Pt–Pd quadrometallic nanoparticles. Nano Converg 6:38. https://doi.org/10.1186/s40580-019-0208-z

Taylor P, Bouziane L, Bendebane F et al (2012) Removal of zinc and cadmium from an aqueous solution using sawdust as a low-cost adsorbent : application of Plackett – Burman design. Desalin Water Treat 49:189–199. https://doi.org/10.1080/19443994.2012.719318

Touihri M, Guesmi F, Hannachi C et al (2021) Single and simultaneous adsorption of Cr(VI) and Cu (II) on a novel Fe3O4/pine cones gel beads nanocomposite: experiments, characterization and isotherms modeling. Chem Eng J 416:129101. https://doi.org/10.1016/j.cej.2021.129101

Vicente-Martínez Y, Caravaca M, Soto-Meca A, Solana-González R (2020) Magnetic core-modified silver nanoparticles for ibuprofen removal: an emerging pollutant in waters. Sci Rep 10:1–10. https://doi.org/10.1038/s41598-020-75223-1

Wei Z, Wang Z, Yan J et al (2019) Adsorption and oxidation of arsenic by two kinds of B-MnO2. J Hazard Mater 373:232–242. https://doi.org/10.1016/j.jhazmat.2019.03.071

Zare F, Ghaedi M, Daneshfar A et al (2015) Efficient removal of radioactive uranium from solvent phase using AgOH–MWCNTs nanoparticles: kinetic and thermodynamic study. Chem Eng J 273:296–306. https://doi.org/10.1016/j.cej.2015.03.002

Zhang J, Li Y, Wang L et al (2015) Catalytic oxidation of formaldehyde overmanganese oxides with different crystal structures. Catal Sci Technol 5:2305–2313. https://doi.org/10.1039/c4cy01461h

Zhao X, Hou Y, Wang Y et al (2017) Prepared MnO2 with different crystal forms as electrode materials for supercapacitors: experimental research from hydrothermal crystallization process to electrochemical performances. RSC Adv 7:40286–40294. https://doi.org/10.1039/c7ra06369e